# Mapping the effect of substrate temperature inhomogeneity during microwave plasma-enhanced chemical vapour deposition nanocrystalline diamond growth

William G.S. Leigh [a,b,*], Jerome A. Cuenca [a], Evan L.H. Thomas [a], Soumen Mandal [a], Oliver A. Williams [a]

[a] *School of Physics and Astronomy, Cardiff University, Cardiff, UK*
[b] *EPSRC Centre for Diamond Science and Technology, UK*

A R T I C L E   I N F O

A B S T R A C T

It is important to account for variance in substrate temperature during microwave plasma-enhanced chemical vapour deposition (MPECVD) nanocrystalline diamond growth, as this has a significant impact on the uniformity of the grown film. In this work, an in-situ method of mapping the substrate temperature under MPECVD growth conditions is demonstrated, employing a mirror galvanometer to scan the field of view of a dual-wavelength pyrometer across the substrate. Temperature maps generated were compared to plasma electron densities simulated using a finite element model. An increase in temperature and simulated plasma density were seen towards the centre of the holder. The properties of nanocrystalline diamond films were mapped using ex-situ Raman spectroscopy and spectroscopic ellipsometry (SE). A greater SE-measured bulk thickness and bulk $sp^3$ fraction, as well as a greater first-order diamond Raman intensity and lower full width at half maximum were seen in the higher-temperature central region, demonstrating the impact of substrate temperature inhomogeneity during growth. The temperature mapping technique demonstrated allows easy evaluation of the impact of substrate holder design, microwave power and chamber pressure on substrate temperature homogeneity, and therefore optimisation of growth conditions for uniform diamond film growth.

## 1. Introduction

The substrate temperature during microwave plasma-enhanced chemical vapour deposition (MPEVCD) nanocrystalline diamond growth has a significant influence on the properties of the deposited film. Growth at lower temperatures has been observed to result in a higher $sp^2$ volume fraction [1], whilst higher substrate temperature results in a higher growth rate [2]. A non-uniform substrate temperature will therefore result in the growth of an inhomogeneous film. This is a particular issue for the scalability of MPECVD diamond growth for applications such as photodetectors [3], boron-doped diamond electrodes [4] and diamond-on-GaN heat management technology [5,6]. Evaluation of the uniformity of substrate temperature is important to allow for optimisation of growth conditions.

Several different techniques have been employed to evaluate substrate temperature uniformity. Zimmer et al. [7] measured the temperature variation across a wafer in a hot filament reactor using 12 thermocouples bonded to the surface, finding that the observed temperature variations corresponded with non-uniformity of film thickness. Whilst this technique is useful in a hot filament reactor, the harsh plasma environment during MPECVD diamond growth makes it impractical to place thermocouples on the surface of the substrate. Placing them on the back of the substrate avoids this issue, but results in the thermocouples sitting between the substrate and water-cooled stage, adding a significant source of uncertainty in the measured temperature.

In general, the preferred substrate temperature measurement technique during MPECVD is pyrometry, either single-colour or dual-wavelength. A single-colour pyrometer determines the temperature of a sample using Wien's approximation of Planck's law:

$$T = \frac{C_2}{\ln\left(\frac{C_1 \varepsilon_\lambda}{\lambda^5 I_\lambda}\right)} \tag{1}$$

---

where T is the temperature of the sample, $C_1$ and $C_2$ are the first and second radiation constants, $I_\lambda$ is the intensity emitted by the sample at the effective wavelength of the pyrometer λ, and $\varepsilon_\lambda$ is the emissivity of the sample at wavelength λ.

This technique was employed by Zuo et al. [8] to investigate the temperature uniformity in a CVD reactor consisting of a 2.45 GHz cavity applicator inside a 12 cm diameter fused bell jar. With emissivity of the pyrometer set to 0.6, the temperature variation across the substrate was probed at a range of microwave power and chamber pressure conditions. It was observed that both temperature at the centre of the substrate and the degree of temperature variation across the substrate increased at higher power and pressure. The notable disadvantage of this form of pyrometry is its dependence on the emissivity of the substrate, as the changes in emissivity of the substrate seen during the growth process can result in significant errors in the measured temperature [9,10].

This problem of changing emissivity can be avoided with the employment of a dual-wavelength (or two-colour) pyrometer, which uses readings at two different wavelengths to determine the temperature, which is determined from the ratio of the two intensities $R_{12}$:

$$T = \frac{C_2(\lambda_2 - \lambda_1)}{\lambda_1\lambda_2\left(5\ln\left(\frac{\lambda_1}{\lambda_2}\right) - \ln(R_{12}) + \ln\left(\frac{\varepsilon_1}{\varepsilon_2}\right)\right)} \quad (2)$$

Assuming the emissivity at the two wavelengths used is the same, the emissivity term will be equal to zero and therefore the temperature measurement becomes independent of emissivity. This approach was used by Mallik et al. [11,12] to measure the temperature at nine different points of a silicon substrate during growth. A temperature gradient was observed across the substrate, and differences in thickness observed using cross-section scanning electron microscopy correlated with this. Inhomogeneity was also observed through Raman spectroscopy, although this did not appear to correlate with growth temperature. Whilst this work provides useful insight, it is somewhat limited by the small number of points of the substrate measured; with only three points from edge to edge of the wafer in any particular axis measured, it is difficult to properly evaluate the shape of the substrate temperature distribution. A more thorough mapping of the temperature of the entire substrate is necessary to achieve this.

Substrate temperature inhomogeneity has also been investigated through the mapping of film properties alone. Ayres et al. [4] investigated the variance of electrochemical properties of boron-doped diamond wafers grown at varying methane fractions, finding a spatial variance in $sp^2$ content. Other work has combined film property mapping with a computational approach. Cuenca et al. [13] employed a finite element model to investigate the impact of changing substrate holder height on the plasma distribution during growth, comparing simulation results with Raman spectra and SEM images of various regions of the sample and finding good agreement between the two. However, the authors note that the ability to monitor the temperature distribution of a substrate under growth conditions is needed to allow for further optimisation of holder design.

Whilst considerable work into investigating substrate temperature during growth has been carried out previously, up to this point any probing of the substrate temperature distribution under growth conditions has focussed on a small number of isolated points on the substrate, with no ability to map the temperature across the entire substrate.

In this work, an inexpensive and simple to implement non-contact method of measuring of the temperature variation across a substrate under growth conditions is presented, combining existing pyrometric techniques with a mirror galvanometer to produce two-dimensional temperature maps. The limitations of this method are also discussed, with the measured temperature variance compared with simulation data, Raman spectroscopy, and spectroscopic ellipsometry (SE) measurements of grown films.

## 2. Material and methods

A two-dimensional gold mirror galvanometer (galvo) system (Fig. 2) was used to scan the field of view of a WilliamsonIR Pro 92 dual-wavelength pyrometer of nominal spectral response 2 μm through a top-down 2.75″ ConFlat viewport in a Carat Systems CTS6U clamshell-type microwave CVD reactor, producing temperature maps of three different molybdenum substrate holders that are typically used for diamond growth at varying microwave power and chamber pressures. The dimensions and typical usage of the three holders are summarised in Table 1, with schematics shown in Fig. 1. The three holders were selected to ensure that the temperature mapping system can evaluate substrate temperature for various holder designs, as a wide range of holder morphologies are typically used for diamond growth on different substrates. All temperature maps were taken using the maximum extents of the field of view of the galvanometer, which was limited by the geometry of the reactor.

Holder 1 was mapped under a hydrogen plasma with a range of forward microwave power and chamber pressure conditions, summarised in Table 2. Temperature maps were taken in two scan directions; "Y", in which all positions of a single Y-value were mapped before moving on to the next row, and "X", in which all positions of a single X-value were mapped before moving onto the next column. Unless stated otherwise, all scans were taken in the "Y" direction. The step size for all scans was set to 0.2°.

Seeding of silicon substrates is necessary to ensure sufficient nucleation densities for the growth of coalesced films [14,15]. This was carried out by immersing substrates in a monodisperse hydrogen-terminated/DI $H_2O$ colloid and placing this in an ultrasonic bath for 10 min, a technique is known to produce seeding densities in excess of $10^{11}$ $cm^{-1}$ [16].

The second holder was mapped under a hydrogen plasma at various power and pressure conditions, both empty and containing a 2 mm thick, 2″ diameter seeded silicon (100) wafer. These conditions are summarised in Table 3.

To evaluate the effect of the inclusion of methane in the plasma on temperature distribution, a temperature map of the second holder containing an unseeded 2 mm thick silicon wafer was taken under a hydrogen plasma at 4 kW 65 Torr. The wafer was unseeded to eliminate the convolution of temperature readings of the pyrometer with the constructive and destructive interference associated with film growth [17,18]. The feed gas composition was changed to 3% methane diluted in hydrogen, and a second temperature map was taken. The flow of methane was then ceased, and the system was left for 16 h in a hydrogen plasma to ensure the elimination of methane from the reactor, before a third temperature map was taken. A polycrystalline diamond wafer for *ex-situ* Raman characterisation (sample 1) was grown on a seeded silicon wafer of 2 mm thickness in a plasma containing 3% methane diluted in hydrogen, at forward power of 5 kW and chamber pressure of 90 Torr for a period of 86 min. The centre thickness of this wafer was estimated at approximately 600 nm using pyrometric interferometry.

The third holder was used to grow a thin wafer for ex-situ SE

**Table 1**
Summary of the three molybdenum substrate holders used.

| Holder | Dimensions | Typical Usage |
|---|---|---|
| 1 | Cylinder of diameter 40 mm and height 10 mm | Growth on small samples, typically less than 20 × 20 mm |
| 2 | 58 mm diameter, height of 5 mm with 1.5 mm deep recess on top surface and 0.1 mm recess on underside | Thick film growth on 2″ wafers of thickness 2 mm or greater |
| 3 | 76.2 mm diameter, height of 4.2 mm. 51.3 mm diameter 0.4 mm deep recess on top surface, 1.5 mm deep recess on underside | Thin film growth on 2″ wafers of thickness 500 μm. |
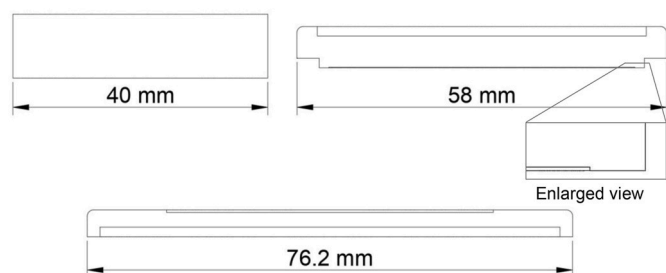
**Fig. 1.** Cross-sections of the three molybdenum substrate holders used. Top left: Holder 1. Top right: Holder 2 with enlarged view of the 0.1 mm recess underneath. Bottom: Holder 3.

characterisation (sample 2). The film was grown on a 500 μm thick, 2″ diameter seeded silicon (100) wafer, at 4.5 kW and 57 Torr, with a 3-min incubation period at 5% methane to prevent etching of the seeds. The methane level during growth was set at 0.4% to maintain a slow growth rate, and therefore reduce the effect of pyrometric interferometry on temperature mapping. Temperature was mapped in the "Y" scan direction, and a second scan in the "X" direction was taken to evaluate whether pyrometric interferometry had significantly affected the apparent temperature. Attempts to map the temperature of the holder containing a 500 μm thick silicon wafer under a solely hydrogen plasma resulted in cracking of the wafer, likely due to etching of the wafer by the plasma.

A J. A. Woollam M-2000D rotating compensator ellipsometer was used for characterisation of sample 2 using SE, at an incidence angle of 70° and wavelength range between 193 and 1000 nm. A motorised tilt/translation stage was used to allow for sample mapping. The resulting spectra were compared to spectra modelled using CompleteEASE software, and an iterative fitting process was carried out, varying modelled sample structure to minimise the mean square error (MSE) between measured and simulated spectra.

Raman spectroscopy was performed using a HORIBA LabRAM spectrometer at an excitation wavelength of 532 nm. A motorised XYZ stage was used to map the intensity of the diamond Raman peak at 1333 $cm^{-1}$. A line scan of the intensity of the diamond Raman peak across the thin sample grown for characterisation by SE was also taken.

To further understand the temperature variation over the sample, a

finite element model (FEM) of the reactor was used, detailed in Ref. [13] In short, the model is built in COMSOL Multiphysics® and simulates the electric field distribution of the cavity, the plasma fluid distribution and the heat transfer solution for a simplified hydrogen plasma model [19] using a cross-section from the Itikawa database [20].

## 3. Results and discussion

### 3.1. Holder 1

Fig. 3 and Fig. 4 show temperature maps of the first holder at a range of power and pressure conditions under a hydrogen plasma. Unsurprisingly, higher power and pressure resulted in greater substrate temperatures (Figs. 3 and 4). Temperatures measured using the galvanometer did not differ substantially from those measured without it. The greatest temperature was observed around the edges of the holder for all conditions, consistent with observations of the edges of the holder

**Table 2**
Conditions used for temperature mapping of holder 1.

| Microwave Power (kW) | Chamber Pressure (Torr) | Substrate |
| --- | --- | --- |
| 3 | 45 | None |
| 3.5 | 75 | None |
| 5 | 90 | None |

**Table 3**
Conditions used for temperature mapping of holder 2.

| Microwave Power (kW) | Chamber Pressure (Torr) | Substrate |
| --- | --- | --- |
| 3 | 45 | None |
| 4 | 65 | None |
| 4.5 | 70 | None |
| 5 | 90 | None |
| 3 | 45 | Seeded 2 mm thick 2″ Si (100) wafer |
| 4 | 65 | Seeded 2 mm thick 2″ Si (100) wafer |
| 4.5 | 70 | Seeded 2 mm thick 2″ Si (100) wafer |
| 5 | 90 | Seeded 2 mm thick 2″ Si (100) wafer |
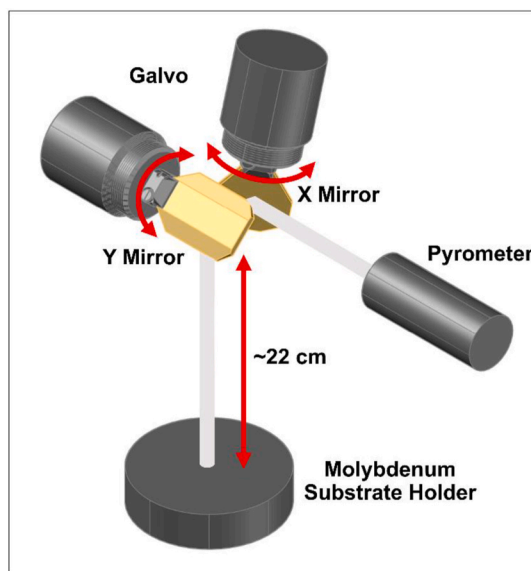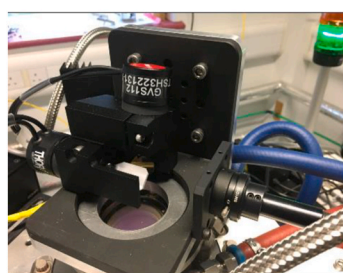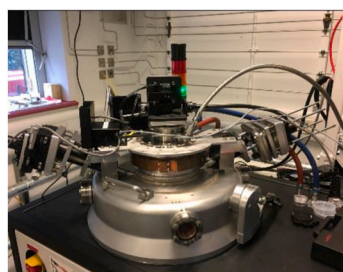


**Fig. 2.** Top left: Clamshell-type reactor with galvo mounted to the top window. Bottom left: Closer look of galvo mounting system. Right: Schematic of galvo scanning system. The white beam illustrates the field of view of the pyrometer. (A colour version of this figure can be viewed online.)
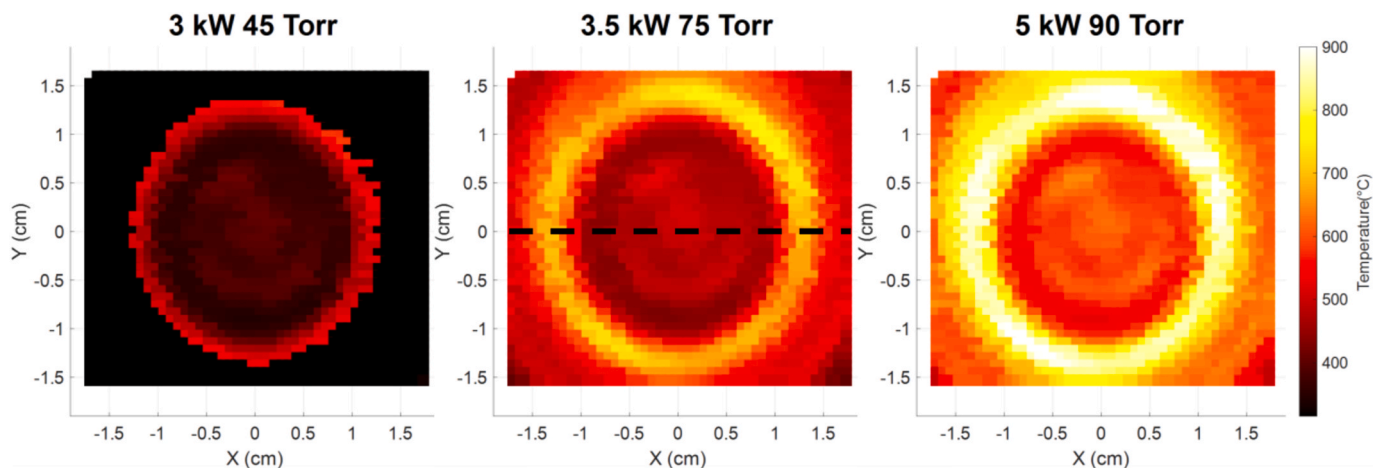
**Fig. 3.** Temperature maps of the first holder under a hydrogen plasma at different power and pressure conditions. The dashed line indicates the region of the holder used for line scans of temperature. (A colour version of this figure can be viewed online.)
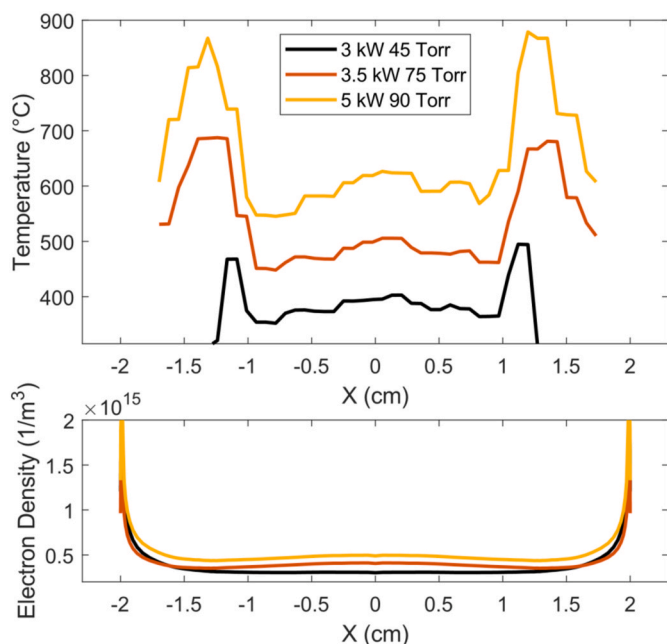


**Fig. 4.** Above: Line scans across the centre of the first holder at Y = 0 (region indicated by the dashed line in Fig. 3) at varying power and pressure conditions. Below: Simulation of the plasma density across the same region. (A colour version of this figure can be viewed online.)

glowing under plasma conditions due to the formation of a secondary plasma around the edge of the holder. Using these glowing edges as reference, a significant limitation is highlighted in that there is an obvious spatial distortion; the sample holder is observed to be approximately 30 mm in diameter as opposed to the actual diameter of 40 mm. This is due to the spot size of the pyrometer (10 mm at the distance used). With the system aimed at the edge of the holder, there is only partial view of the target. In this case, the apparent temperature can read artificially low.

This spatial distortion becomes clear when compared with the FEM result under the same conditions. However, a similar effect is seen in the model where the edges of the sample holder are hotter than the centre. This is attributed to the high electric field at the edges of the puck, thereby focusing the plasma around here. Additionally, the centre of the sample is at a marginally elevated temperature which is also corroborated with the model and is simply due to the plasma ball being centred

in the middle of the cavity.

### 3.2. Holder 2

Fig. 5 shows temperature maps of the second holder under a hydrogen plasma at a range of power and pressure conditions, both empty and containing a 2" diameter, 2 mm thick Si (100) wafer seeded with hydrogen-terminated nanodiamond. Fig. 6 shows a comparison of temperature distribution along a line across the centre of the holder at Y = 0, along with plots of the simulated plasma density in the same region.

As with holder 1, the greatest temperatures were seen around the edges of the holder, consistent with observations of the edges of the holder glowing. Again, these observations were attributed to the higher electric field at the edge of the holder resulting in the formation of a secondary plasma around the edges of the holder. Unlike holder 1, there was no region of elevated temperature at the centre of the holder, despite an increase in simulated plasma density in this region. It is believed that this is a result of the morphology of the holder. It contains a 1.5 mm deep recess at the centre, and therefore does not protrude as much towards the centre of the plasma ball, resulting in less heating. Also seen is a region of lower temperature towards the edges of the holder, just before the spike in temperature at the edge. This is also believed to be an artefact of holder shape. Holder 2 does not contact the water-cooled reactor stage throughout its entire diameter in order to reduce cooling and allow for the high substrate temperatures at lower power and pressure (in excess of 700 °C) typically required for high quality diamond film growth [1,17,21–23]. Contact with the reactor stage is only through a narrow (1.5 mm wide) ring close to the edge of the holder, and the resultant non-uniform cooling is thought to be responsible for this aspect of the observed temperature distribution.

With the placement of a 2 mm-thick seeded 2" silicon wafer in the holder, a region of elevated temperature was again seen in the centre of the substrate. As the recess in the holder is 1.5 mm deep, the wafer stands 0.5 mm proud from the top surface of the holder, and therefore protrudes further towards the plasma ball, resulting in more heating. At the centre, the temperature increase between an empty and non-empty holder was between 120 and 222 °C, greater for higher power and pressure. A similar increase in temperature was seen at the edges of the holder. Whilst simulated plasma density across the central region is very similar for both the empty and non-empty holder, there is a divergence around the edges; whilst an increase in plasma density is seen at the edge of the holder containing an Si wafer, this is less pronounced than with the empty holder.

Up to this point, temperature mapping was carried out under a plasma containing only hydrogen to prevent diamond film growth.
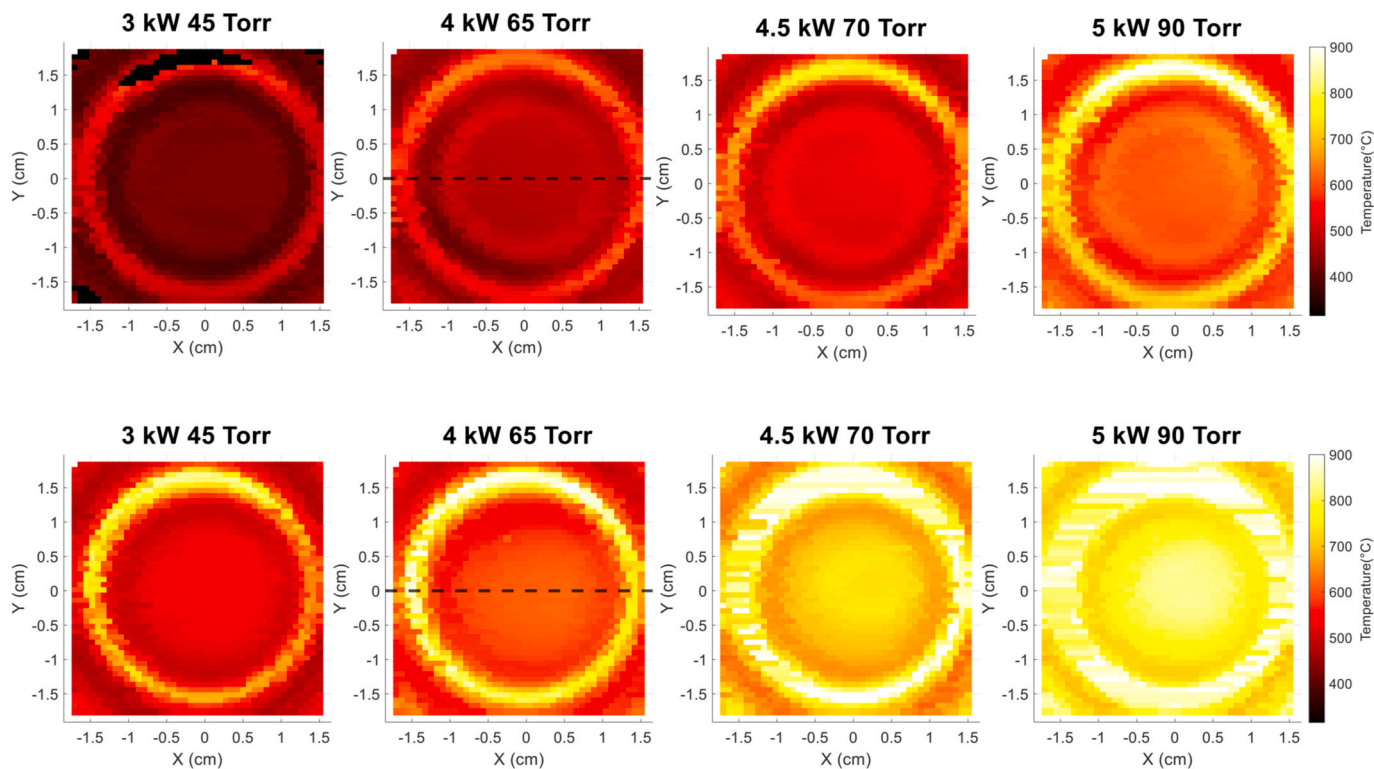
**Fig. 5.** Above: Temperature maps of the empty second holder under a hydrogen plasma at different power and pressure conditions. Below: Temperature maps of the larger wafer holder containing a seeded 2 mm thick, 2″ diameter Si (100) wafer at various power and pressure conditions under a hydrogen plasma. The dashed line indicates the region used for line scans. (A colour version of this figure can be viewed online.)
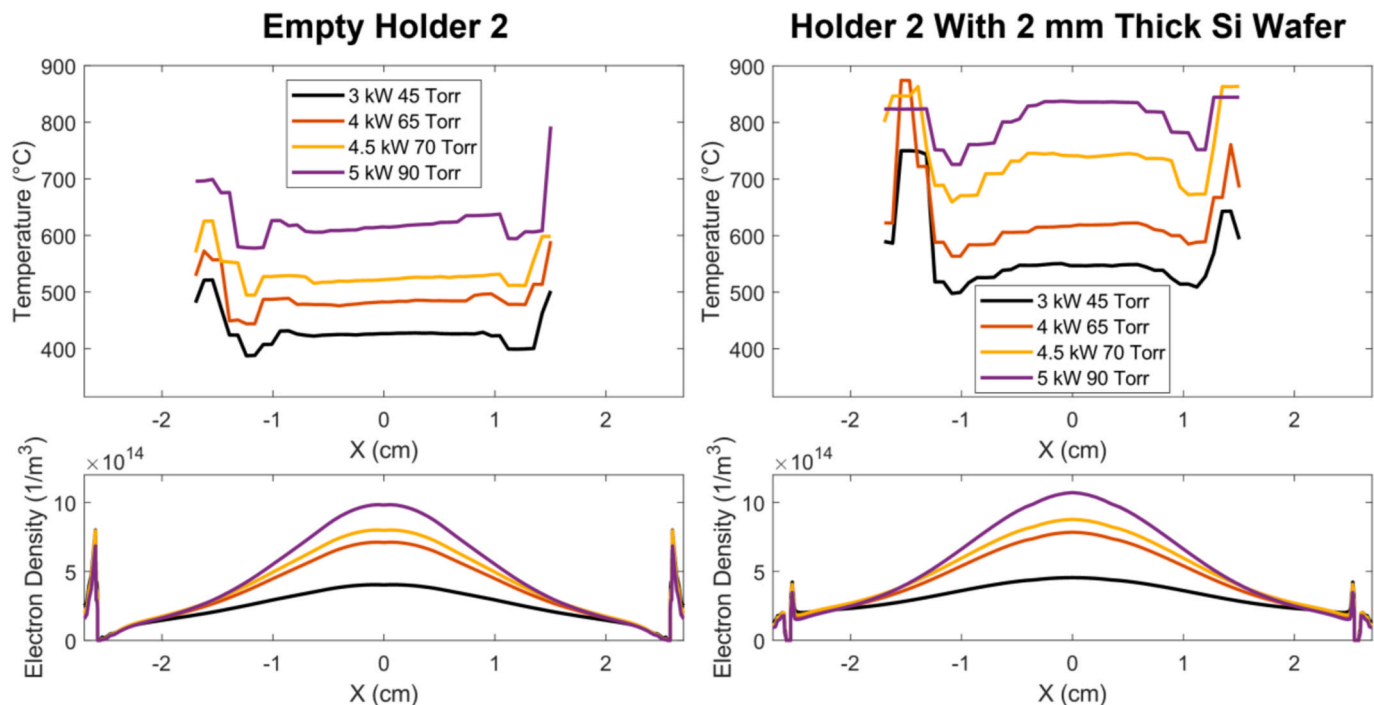


**Fig. 6.** Above: Comparison of temperature line scans across the centre of the empty second holder (left) and the second holder at Y = 0 (region indicated by the dashed line in Fig. 5) containing a 2 mm-thick seeded 2″ silicon wafer (right) at various power and pressure conditions under a hydrogen plasma. Below: Simulation of the plasma density across the same region of each holder. (A colour version of this figure can be viewed online.)

During film growth, the apparent pyrometer temperature measured will oscillate over time due to interference from varying thickness of the film [18,24], and growth could therefore result in inaccurate temperature maps. It is therefore important to assess the effectiveness of the use of a hydrogen plasma to approximate MPECVD diamond growth conditions.

To evaluate this, a sequence of temperature maps of holder 2

containing an unseeded 2 mm-thick Si (100) wafer were taken; the first of which under a hydrogen plasma, the second in a plasma comprising 3% methane diluted in hydrogen (typical for MPECVD diamond growth [21–23]), and the third after being left under a hydrogen plasma for 16 h to ensure the elimination of methane from the chamber. The duration of the time in the methane plasma was 55 min. Addition of methane resulted in an increase in temperature of approximately 50 °C at the centre of the substrate as a result of heat released by the reaction between CH and H species [25]. Whilst the measured temperature increased, the shape of the temperature distribution did not change, as this increase was uniform across the entire central region of the substrate. This suggests that temperature mapping under a hydrogen plasma is a reasonable approximation for the shape, but not the magnitude, of the temperature distribution under growth conditions.

Removal of methane from the plasma did not result in a significant decrease in temperature across the centre of the substrate, but a decrease was seen around the edge of the holder. Lack of temperature decrease in the centre is likely due to the observed etching of the silicon substrate; the emissivity of silicon is influenced by surface roughness [26], which in turn will change the apparent temperature measured by a pyrometer.

Raman spectroscopy was used to evaluate the effect of temperature inhomogeneity during growth on both the thickness and quality of the film. Previous studies have shown that higher growth temperatures can result in both a faster growth rate and a lower $sp^2$ volume fraction [1,2]. Across the entire wafer, a sharp peak at 1333 $cm^{-1}$ (Full width at half maximum [FWHM] 7.7 $\pm$ 0.2 $cm^{-1}$ in the centre of the film) was seen in the Raman spectrum, attributed to the first order diamond Raman peak

and indicative of a high-quality diamond film [27]. The position of this peak was unchanged across the sample.

Fig. 7 compares Raman of sample 1 with the temperature map of a 2 mm thick Si wafer under a hydrogen plasma at the same microwave power and reactor pressure used for growth of the thicker sample, with Fig. 8 showing representative Raman spectra from different regions of the film. The greatest Raman intensity was seen in the central region of the diamond film, decreasing towards the edges, showing a similar pattern to the measured temperature. It is worth noting that the laser can penetrate the entire 600 nm-thick film, so the thickness of the film will have a significant influence on the intensity of the diamond Raman peak. The greater intensity in the centre is therefore indicative of both a higher quality and thicker film in this region.

The FWHM of the diamond Raman peak can be used to provide a qualitative indication of film quality, as a higher level of defects within the film will result in broadening of the peak [28,29]. The FWHM of the diamond Raman peak was lowest in the centre of the film, increasing towards the edge, suggesting that the higher substrate temperature in the centre results in a higher quality film.

### 3.3. Holder 3

Initial attempts at mapping the temperature of the third holder containing a seeded 500 μm thick Si wafer under a hydrogen plasma resulted in fracturing of the wafer. This appears to have been due to etching of the wafer by the hydrogen plasma, with etch pits visible on the wafer shards. Mapping was carried out at a low methane
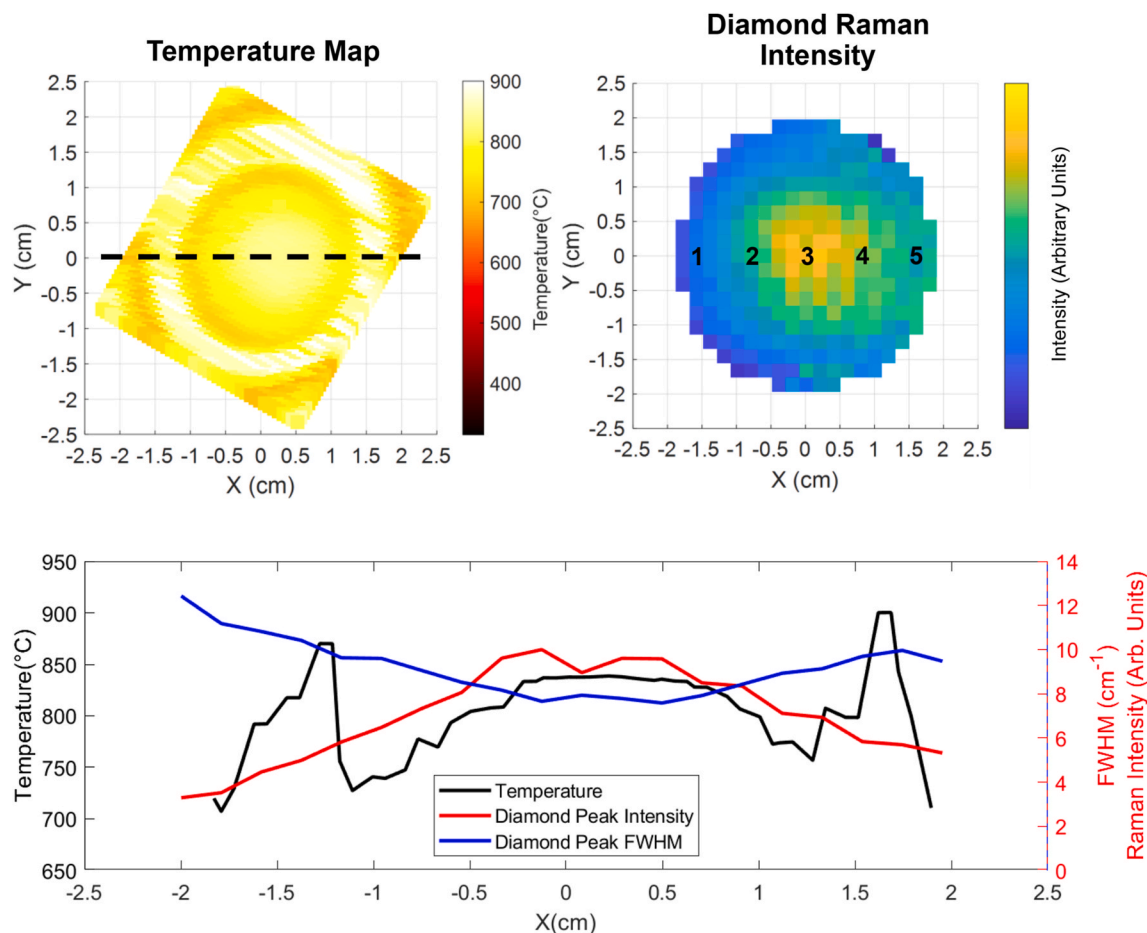


**Fig. 7.** Above, from left: Temperature map of the substrate holder containing a 2 mm thick Si wafer under a hydrogen plasma at 5 kW 90 Torr, rotated to match the orientation of the property maps; Map of the intensity of the first order diamond Raman peak at 1333 $cm^{-1}$. Below: Line scans across the region of the film indicated by the dashed line in the temperature map: Temperature line scan under a hydrogen plasma; Intensity of the first order diamond Raman peak at 1333 $cm^{-1}$; FWHM of the first order diamond Raman peak at 1333 $cm^{-1}$. (A colour version of this figure can be viewed online.)
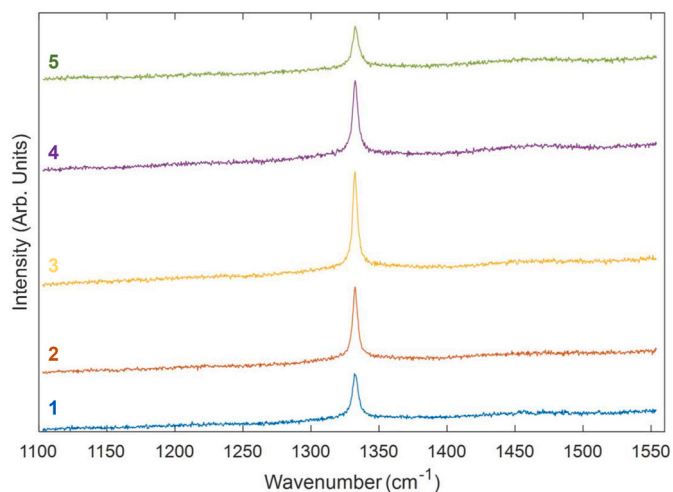
**Fig. 8.** Representative Raman spectra from the positions of sample 1 indicated in Fig. 7. (A colour version of this figure can be viewed online.)

concentration (0.4%), resulting in slow diamond film growth to prevent etching of the Si substrate. Fig. 9 shows temperature maps of the third holder under these conditions. To verify that the film growth rate was slow enough to prevent pyrometric interferometry disrupting the temperature map, two sequential scans were taken in the two different scan directions. The temperature maps of these scans were almost identical, indicating that pyrometric interferometry did not have a substantial impact on the mapping.

An additional limitation of the measurement technique for this reactor was presented when mapping the third holder; as the third holder is larger in diameter than the first two, the geometry of the reactor meant that the edges of the third holder extended out of the field of the view of the temperature mapping system. The area of greatest temperature around the edge seen with the other two holders was only visible in the bottom left corner of the temperature map. Notably, the region of the holder containing the Si wafer was entirely within the field of view of the mapping system. There was no significant difference between the two sequential temperature maps, indicating that the growth rate was not fast enough to result in distortion of the temperature mapping by pyrometric interferometry. As seen previously with the other two holders, the greatest temperature was seen in the centre of the substrate, decreasing towards the edges.

The thin nature of sample 2 (approx. 60 nm thick in the centre) allowed for characterisation using SE. Most previous use of ellipsometry to characterise polycrystalline diamond films utilises a Bruggeman effective medium approximation (EMA) to combine the optical constants of anticipated components of the film [30–32]. Generally, two additional components are added to diamond in this bulk layer, void, and $sp^2$ carbon. Given that the precise optical constants of $sp^2$ content within polycrystalline are not easily quantifiable, it is necessary to use those of another material, such as glassy carbon, to approximate them [32].

Characterisation of thicker nanocrystalline diamond films presents several difficulties. The effective medium approximation used to model the bulk layer is only valid where the size of phases are smaller than one tenth of the probing wavelength [33]. Additionally, surface roughness resulting from the overgrowth of competing crystallites can lead to
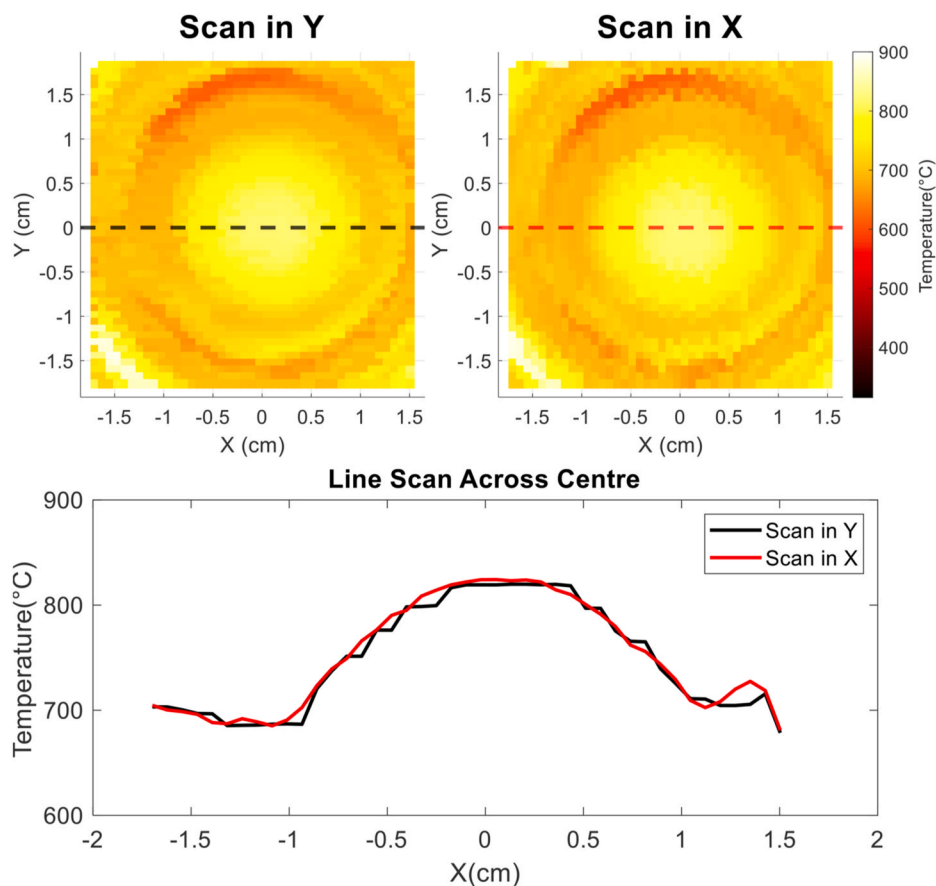


**Fig. 9.** Above: Sequential scans of holder 3 containing a seeded 500 μm thick Si wafer under a plasma consisting of 0.4% methane diluted in hydrogen in the "Y" scan direction (left) and in the "X" scan direction (right). Below: Line scans across the region of the holder indicated by the dashed line. (A colour version of this figure can be viewed online.)

scattering of the incident light, leading to depolarisation [33,34]. These issues were evident in the initial analysis of spectra taken between 193 and 1000 nm. Use of a model previously shown to effectively characterise early-stage diamond films [32] resulted in a significant mean square error (MSE) between simulated and measured spectra. The model comprises a three layer stack atop a silicon substrate, with reference optical constants of silicon [35] used for the substrate. The next layer used optical constants of cubic silicon carbide [36] to represent the carburisation of silicon substrates previously observed to occur during CVD diamond growth [37,38]. The bulk polycrystalline diamond layer was represented using an EMA with three components; a general oscillator matched to reference optical constants of diamond [39], void, and optical constants of glassy carbon [40] to represent $sp^2$ carbon. The final layer was an EMA consisting of 50% bulk layer and 50% void to approximate surface roughness. It was observed that there was a high level of correlation between the thickness of the SiC layer and other parameters, including surface roughness and bulk layer thickness. As a result of this, the thickness of this layer was not allowed to vary across the whole film and was instead fixed at the 1.75 nm measured in the centre of the film.

The films previously characterised using this model were thinner than the film characterised in this work [32]. To reduce the impact of scattering due to surface roughness, the minimum wavelength was increased to 300 nm, resulting in a significant reduction in MSE. In the final iteration of the model, the only quantities allowed to vary through the fit process were the surface roughness and the thickness and composition of the bulk layer. To account for depolarisation, an instrument bandwidth of 5 nm was incorporated into the model.

Fig. 10 compares maps of the SE-derived properties and MSE with the temperature map of the sample during growth, whilst Fig. 11 shows line scans across the centre of the wafer of the SE-derived properties and temperature with the intensity of the first-order diamond Raman peak in the same region. Representative Raman spectra from various regions of the sample are shown in Fig. 12. Due to the limited thickness of sample 2

(60 nm measured by SE in the centre of the film), long laser exposure times were required to generate sufficient signal for Raman characterisation. As a result of this, Raman mapping of the sample was restricted to a line scan across the centre. The region of greatest temperature in the centre of the wafer corresponded with the greatest SE-measured bulk thickness. As noted earlier, it has previously been seen that higher substrate temperatures result in faster growth rates [2]. The inverse trend was seen in the levels of bulk impurity in the diamond film; the glassy carbon (approximating $sp^2$ material) and void fractions were lowest in the centre, increasing towards the edges. This matches previous SE measurements suggesting that a greater proportion of $sp^2$ material is incorporated in the early stages of film growth at lower substrate temperatures [1]. An area of very low bulk thickness was observed in the top left of the sample, resulting from delamination of the film there.

As with sample 1, the intensity of the first-order diamond Raman peak at 1333 $cm^{-1}$ was greatest in the high-temperature central region, decreasing towards the edge. Given that sample 2 is very thin, the intensity of this peak will be impacted by the thickness as well as the quality of the film, as the laser is easily capable of penetrating through the entire film. A thicker film will result in a more intense peak, as will a higher-quality film. This observation correlates with the SE model showing both greater bulk thickness and a greater proportion of $sp^3$ content (and therefore higher quality film) in the centre.

### 4. Conclusions

Substrate temperature inhomogeneity under MPECVD growth conditions was investigated *in-situ* using a mirror galvanometer, scanning the field of view of a dual-wavelength pyrometer to produce temperature maps. An increase in temperature was seen towards the centre of the holder, matching finite element simulations of a greater plasma density in this region. Similarly, the observation of high temperature around the edge of the holders was validated with high plasma density in this area. The properties of diamond films were mapped using *ex-situ*
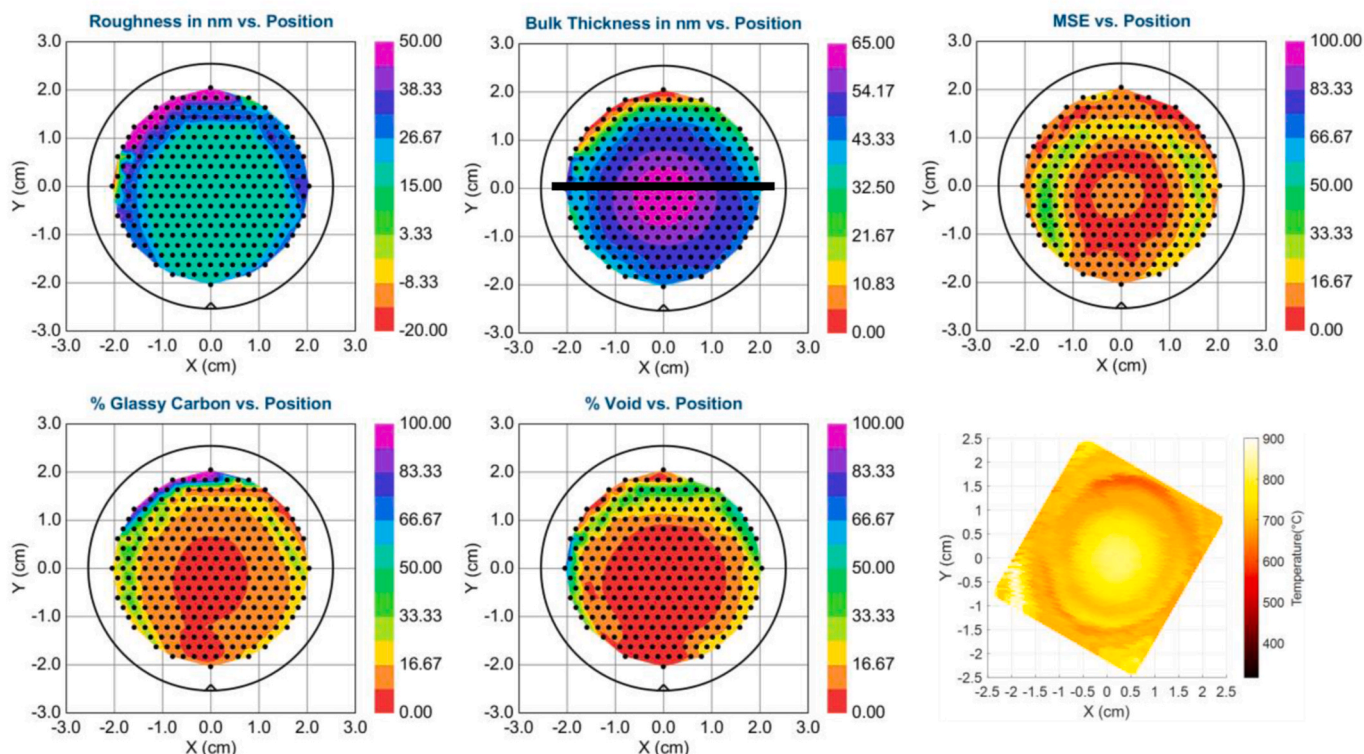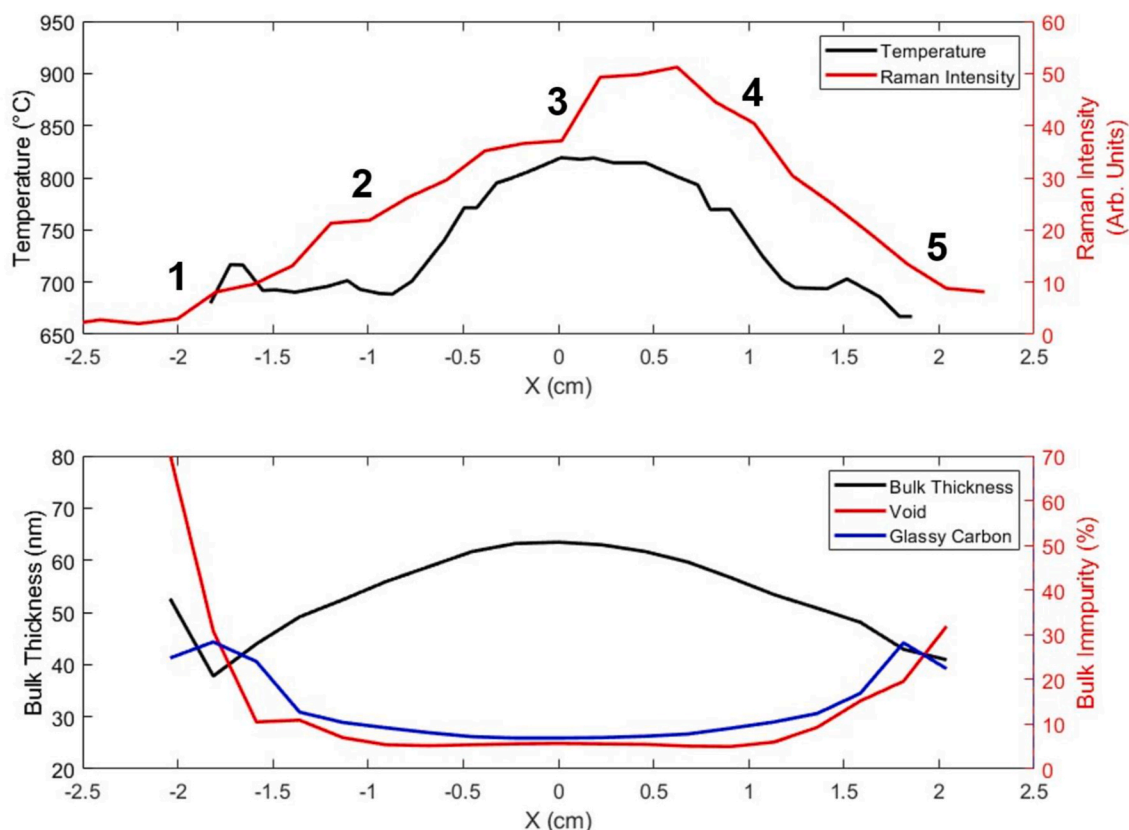


**Fig. 10.** Clockwise, from top left: Thickness of surface roughness layer in the SE model across sample 2; thickness of the bulk EMA layer; MSE of the model; temperature map of the sample during growth, rotated to match the orientation of the SE spectra; bulk EMA void fraction; bulk EMA glassy carbon fraction.

**Fig. 11.** Line scans across the centre of sample 2 at Y = 0 (region indicated by the solid line in Fig. 10). Above: Temperature during growth; intensity of the first order diamond Raman peak at 1333 cm$^{-1}$. Below: SE-derived bulk layer thickness and bulk impurity fractions. (A colour version of this figure can be viewed online.)
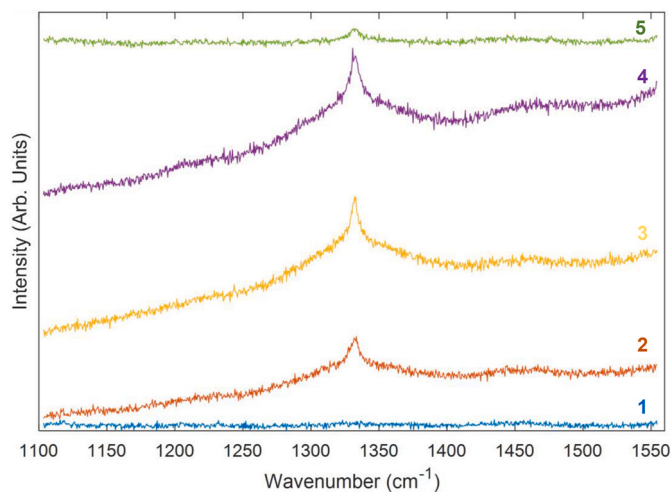


**Fig. 12.** Representative Raman spectra from the region of sample 2 indicated in Fig. 11.

Raman spectroscopy and SE and compared with temperature maps at the same power and pressure. A greater SE-measured bulk thickness and bulk sp$^3$ fraction were seen in the central region of higher temperature, as was a greater intensity and lower FWHM of the first-order diamond Raman peak, indicative of a thicker and higher-quality film. The correlation between mapped temperature, simulated plasma density and thickness and composition of diamond films demonstrates that this technique is an effective measurement of substrate temperature distribution. Given that ensuring film uniformity is a significant challenge to diamond growth, the ability to map the substrate temperature is a powerful tool to evaluate the impact of substrate holder design, microwave power and chamber pressure allowing for further optimisation of growth conditions.

**CRediT authorship contribution statement**

**William G.S. Leigh:** Conceptuzlisation, Methodology, Software, Formal analysis, Investigation, Writing – original draft, Writing – review & editing, Visualization. **Jerome A. Cuenca:** Software, Formal analysis, Investigation, Writing – review & editing, Supervision. **Evan L.H. Thomas:** Investigation, Writing – review & editing, Supervision. **Soumen Mandal:** Investigation, Writing – review & editing, Supervision. **Oliver A. Williams:** Resources, Writing – review & editing, Supervision, Project administration, Funding acquisition.

**Declaration of competing interest**

The authors declare that they have no known competing financial interests or personal relationships that could have appeared to influence the work reported in this paper.

**Data availability**

Information on the data underpinning the results presented here, including how to access them, can be found in the Cardiff University data catalogue at http://doi.org/10.17035/d.2022.0218580664.

Training in Diamond Science and Technology (EP/L015315/1).

## References

[1] B. Hong, et al., Effects of processing conditions on the growth of nanocrystalline diamond thin films: real time spectroscopic ellipsometry studies, Diam. Relat. Mater. 6 (1997) 55–80.

[2] T.G. McCauley, D.M. Gruen, A.R. Krauss, Temperature dependence of the growth rate for nanocrystalline diamond films deposited from an Ar/CH4 microwave plasma, Appl. Phys. Lett. 73 (1998) 1646–1648.

[3] E. Pace, A. De Sio, Diamond detectors for space applications, Nucl. Instrum. Methods Phys. Res. Sect. A Accel. Spectrom. Detect. Assoc. Equip. 514 (2003) 93–99.

[4] Z.J. Ayres, et al., Impact of chemical vapour deposition plasma inhomogeneity on the spatial variation of sp2 carbon in boron doped diamond electrodes, Carbon 121 (2017) 434–442.

[5] J.W. Pomeroy, et al., Contactless thermal boundary resistance measurement of GaN-on-Diamond wafers, IEEE Electron. Device Lett. 35 (2014) 1007–1009.

[6] M.D. Smith, et al., GaN-on-diamond technology platform: bonding-free membrane manufacturing process, AIP Adv. 10 (2020), 035306.

[7] J. Zimmer, K.V. Ravi, Aspects of scaling CVD diamond reactors, Diam. Relat. Mater. 15 (2006) 229–233.

[8] S.S. Zuo, M.K. Yaran, T.A. Grotjohn, D.K. Reinhard, J. Asmussen, Investigation of diamond deposition uniformity and quality for freestanding film and substrate applications, Diam. Relat. Mater. 17 (2008) 300–305.

[9] P. Spiberg, R.L. Woodin, J.E. Butler, L. Dhar, In-situ Fourier transform IR emission spectroscopy of diamond chemical vapor deposition, Diam. Relat. Mater. 2 (1993) 708–712.

[10] M.T. Bieberich, S.L. Girshick, Control of substrate temperature during diamond deposition, Plasma Chem. Plasma Process. 16 (1995) S157–S168.

[11] A.K. Mallik, et al., Influence of the microwave plasma CVD reactor parameters on substrate thermal management for growing large area diamond coatings inside a 915 MHz and moderately low power unit, Diam. Relat. Mater. 30 (2012) 53–61.

[12] A.K. Mallik, et al., Property mapping of polycrystalline diamond coatings over large area, J Adv Ceram 3 (2014) 56–70.

[13] J.A. Cuenca, S. Mandal, E.L.H. Thomas, O.A. Williams, Microwave plasma modelling in clamshell chemical vapour deposition diamond reactors, Diam. Relat. Mater. 124 (2022), 108917.

[14] O.A. Williams, Nanocrystalline diamond, Diam. Relat. Mater. 20 (2011) 621–640.

[15] S. Mandal, Nucleation of diamond films on heterogeneous substrates: a review, RSC Adv. 11 (2021) 10159–10182.

[16] J. Hees, A. Kriele, O.A. Williams, Electrostatic self-assembly of diamond nanoparticles, Chem. Phys. Lett. 509 (2011) 12–15.

[17] O.A. Williams, et al., Comparison of the growth and properties of ultrananocrystalline diamond and nanocrystalline diamond, Diam. Relat. Mater. 15 (2006) 654–658.

[18] K.A. Snail, C.M. Marks, *In situ* diamond growth rate measurement using emission interferometry, Appl. Phys. Lett. 60 (1992) 3135–3137.

[19] H. Yamada, A. Chayahara, Y. Mokuno, Simplified description of microwave plasma discharge for chemical vapor deposition of diamond, J. Appl. Phys. 101 (2007), 063302.

[20] J.-S. Yoon, et al., Cross sections for electron collisions with hydrogen molecules, J. Phys. Chem. Ref. Data 37 (2008) 913–931.

[21] O.A. Williams, et al., High Young's modulus in ultra thin nanocrystalline diamond, Chem. Phys. Lett. 495 (2010) 84–89.

[22] A. Köpf, R. Haubner, B. Lux, Multilayer coatings containing diamond and other hard materials on hardmetal substrates, Int. J. Refract. Metals Hard Mater. 20 (2002) 107–113.

[23] S. Bühlmann, E. Blank, R. Haubner, B. Lux, Characterization of ballas diamond depositions, Diam. Relat. Mater. 8 (1999) 194–201.

[24] F. Bénédic, M. Belmahi, T. Easwarakhanthan, P. Alnot, In situ optical characterization during MPACVD diamond film growth on silicon substrates using a bichromatic infrared pyrometer under oblique incidence, J. Phys. D Appl. Phys. 34 (2001) 1048–1058.

[25] N. Ali, V.F. Neto, J. Gracio, Promoting secondary nucleation using methane modulations during diamond chemical vapor deposition to produce smoother, harder, and better quality films, J. Mater. Res. 18 (2003) 296–304.

[26] S. Abedrabbo, et al., Perspectives on emissivity measurements and modeling in silicon, Mater. Sci. Semicond. Process. 1 (1998) 187–193.

[27] D.S. Knight, W.B. White, Characterization of diamond films by Raman spectroscopy, J. Mater. Res. 4 (1989) 385–393.

[28] M. Pandey, R. D'Cunha, A.K. Tyagi, Defects in CVD diamond: Raman and XRD studies, J. Alloys Compd. 333 (2002) 260–265.

[29] M. Pandey, V. Sugandhi, R. D'cunha, A.K. Sikder, D.S. Mishra, Spectroscopic studies of hydrogen related defects in CVD diamond, Bull. Mater. Sci. 21 (1998) 479–484.

[30] D.E. Aspnes, J.B. Theeten, F. Hottier, Investigation of effective-medium models of microscopic surface roughness by spectroscopic ellipsometry, Phys. Rev. B 20 (1979) 3292–3302.

[31] N. Cella, et al., Ex-situ spectroscopic ellipsometry studies of micron thick CVD diamond films, Diam. Relat. Mater. 5 (1996) 1424–1432.

[32] E.L.H. Thomas, et al., Spectroscopic ellipsometry of nanocrystalline diamond film growth, ACS Omega 2 (2017) 6715–6727.

[33] H. Fujiwara, Spectroscopic Ellipsometry: Principles and Applications, John Wiley & Sons, 2007.

[34] Z. Pápa, J. Budai, I. Hanyecz, J. Csontos, Z. Toth, Depolarization correction method for ellipsometric measurements of large grain size zinc-oxide films, Thin Solid Films 571 (2014) 562–566.

[35] C.M. Herzinger, B. Johs, W.A. McGahan, J.A. Woollam, W. Paulson, Ellipsometric determination of optical constants for silicon and thermally grown silicon dioxide via a multi-sample, multi-wavelength, multi-angle investigation, J. Appl. Phys. 83 (1998) 3323–3336.

[36] E.D. Palik, Handbook of Optical Constants of Solids III, Academic Press, 1998.

[37] J.C. Arnault, et al., Diamond nanoseeding on silicon: stability under H2 MPCVD exposures and early stages of growth, Diam. Relat. Mater. 17 (2008) 1143–1149.

[38] B.R. Stoner, G.-H.M. Ma, S.D. Wolter, J.T. Glass, Characterization of bias-enhanced nucleation of diamond on silicon by invacuo surface analysis and transmission electron microscopy, Phys. Rev. B 45 (1992) 11067–11084.

[39] E.D. Palik, Handbook of Optical Constants of Solids, vol. 3, Acad. Press, 2003.

[40] M.W. Williams, E.T. Arakawa, Optical properties of glassy carbon from 0 to 82 eV, J. Appl. Phys. 43 (1972) 3460–3463.